Electronic Supplementary Material (ESI) for Journal of Materials Chemistry A.

Understanding and Tackling Lattice Manganese Exfoliation and Deactivation of Battery-Type NiMn-LDH in Fast Electrochemical Energy Storage

*Yanqun Tang, Zibin Liang, Yongkang Jin, Song Gao and Ruqiang Zou**

Beijing Key Laboratory for Theory and Technology of Advanced Battery Materials,

Institute of Clean Energy,

School of Materials Science and Engineering,

Peking University, 100871, P. R. China

E-mail: rzou@pku.edu.cn

EXPERIMENTAL DETAILS

Chemicals. $NiCl_2 \cdot 6H_2O$, $MnCl_2 \cdot 4H_2O$, methenamine, H_2O_2, and Polytetrafluoroethylene (PTFE) were purchased from Sinopharm Chemical Reagent. Activated carbon was purchased from XFNANO scientific Ltd. Ketjen Black was purchased from Shanghai Hesen Electric Co. All reagents were of analytical grade and were used without further purification. Ultrapure water was used throughout the experiments. The Ni foam was received from Kunshan Jiayisheng Dianziwang Technology Co., Ltd. The Ni foam was soaked in a solution of 2 M HCl for 10 min to remove the surface oxide layer. Subsequently, it was washed in an ultrasonic bath of acetone for 10 min to eliminate oil splashes. Finally, it was rinsed with ethanol and deionized water 3 times, respectively. The separator for ASC was purchased from Nippon Kodoshi Co., Ltd.

Preparation of NiMn-LDH. NiMn-LDH was synthesized by a simple one-step hydrothermal method. Briefly, $NiCl_2 \cdot 6H_2O$ and $MnCl_2 \cdot 4H_2O$ were dissolved in deionized water to form a 30 mL solution of 0.08 M concentration (Ni^{2+}: Mn^{2+} = 5: 1 molar ratio). 4 mmol methenamine was then added into the above solution. After stirring for 1 hour, the above solution was transferred into a 100mL Teflon-lined stainless-steel autoclave. Hydrothermal growth was conducted at 90 ℃ for 6 h. Finally, the resulting NiMn-LDH was thoroughly washed with water and dried at 70 ℃ for 12 h in a vacuum oven.

Preparation of NiO_xH_y and MnO_xH_y. For comparison, NiO_xH_y and MnO_xH_y were prepared by a similar procedure. Only $NiCl_2 \cdot 6H_2O$ or $MnCl_2 \cdot 4H_2O$ was dissolved as the metal source to form a 0.08 M solution for the deposition of their oxides or hydroxides. The deposition was carried out under the same conditions as above with no addition of another metal source.

Preparation of LDH-O. 500 μL of H_2O_2 (30 %) was diluted to 100 mL to prepare a solution of concentration 0.15 %. 50 mg of NiMn-LDH was added to the above solution, stirred at 700 rpm for 30 minutes. After suction filtration, the resulting LDH-O was thoroughly washed with water and dried at 70 ℃ for 12 h in a vacuum oven.

Characterizations. X-ray photoelectron spectrometry (XPS) was recorded using Al Kα radiation (Thermo Fisher Scientific).

Powder X-ray diffraction (XRD) patterns of all the samples were carried out using a graphite-filtered Cu Kα radiation operating at 40 kV and 30 mA, λ= 0.15418 nm (SmartLab 9KW, Rigaku).

Scanning electron microscopy with an accelerating voltage of 20 kV (SEM, ZeissSUPRA) was

applied for detailed morphology analyses.

TEM and EDS mappings were taken using microscopy (Tecnai F30, FEI, US) combined with an EDX spectroscopy. For TEM observations, the samples were scraped from the Ni foam substrate and ultrasonically dispersed in ethanol and then a drop of the suspension was deposited onto a carbon-coated Cu grid followed by the evaporation of the solvent in air.

Electrochemical measurement: The electrochemical measurements were carried out by using a CHI760E electrochemical workstation in the case of both three-electrode configuration and two-electrode device. For the working electrode of a three-electrode system, a mixture slurry containing 70 wt% active materials, 20 wt% Ketjen Black, and 10 wt% PTFE binder was prepared then rolled with the assistance of ethanol to form a uniform film with a typical areal mass of approximately 2 ~ 3 mg cm^{-2}. The film electrode was then pressed between two nickel foam, and dried under vacuum at 80 ˚C for 12 h. The working electrodes are fully activated in the electrolyte before each test. A platinum mesh electrode and a Hg/HgO electrode were used as the counter and the reference electrodes, respectively. The cyclic voltammograms (CV) were acquired in a potential range between 0 and 0.60 V at different scan rates, and the charge-discharge processes were performed between 0.1 and 0.55 V at different current densities in a 2 M KOH aqueous electrolyte. Based on the galvanostatic discharge curve, the specific capacity Q (C g^{-1}) of the battery-type electrode material was calculated as follows:

$$Q = i_m \Delta t \tag{1}$$

where i_m=I/m (A g^{-1}) is the current density, m is the mass of the active material, Δt (s) is the discharge time.

The specific capacitance C (F g^{-1}) was calculated from the galvanostatic charge-discharge measurements using the following equation,

$$C = \frac{2i_m \int V dt}{V^2 \big|_{V_i}^{v_f}} \tag{2}$$

C represents the galvanostatic discharge specific capacitance. $\int V dt$ is the integral current area, where V is the potential with initial and final values of V_i and V_f, respectively. $i_m = I/m$ is the current density, where I is the current and m is the mass of active materials.

The electrochemical measurements of the two-electrode device containing LDH-O or NiMn-LDH

as the positive electrode and activated carbon as a negative electrode with separator of MPF30AC-100 (Nippon Kodoshi Corporation, Kochi, Japan) in a split test cell (Hefei Kejing Co.) configuration were carried out in a 2 M KOH electrolyte. The mass ratio of the positive electrode to the negative electrode is determined according to charge balance theory ($q+ = q-$). Based on the CV results from the three-electrode system,

$$q = \int imdV/v \tag{3}$$

where q represents the charge, m is the mass of the active material, and $\int idV/v$ is the integral area from CV.

In order to achieve charge balance, $m^+ \cdot \left(\int \frac{idV}{v}\right)_+ = m^- \cdot \left(\int \frac{idV}{v}\right)_-$, thus,

$$R = m^+ : m^- = \left(\int \frac{idV}{v}\right)_- : \left(\int \frac{idV}{v}\right)_+ \tag{4}$$

The CV was acquired in a potential range between 0 and 1.6 V at different scan rates, and the charge-discharge processes were performed by cycling the potential from 0 to 1.55 V at different current densities.

The energy density E (Wh kg^{-1}) and power density P (kW kg^{-1}) in the Ragone plot were calculated with the following equations,

$$E = \frac{1}{2} \cdot \frac{C \cdot \Delta V^2}{3.6} \tag{5}$$

$$P = 3.6 \cdot \frac{E}{\Delta t} \tag{6}$$

Where C is the specific gravimetric capacitance (F g^{-1}), ΔV is the potential window (V), and Δt is the discharge time (s).

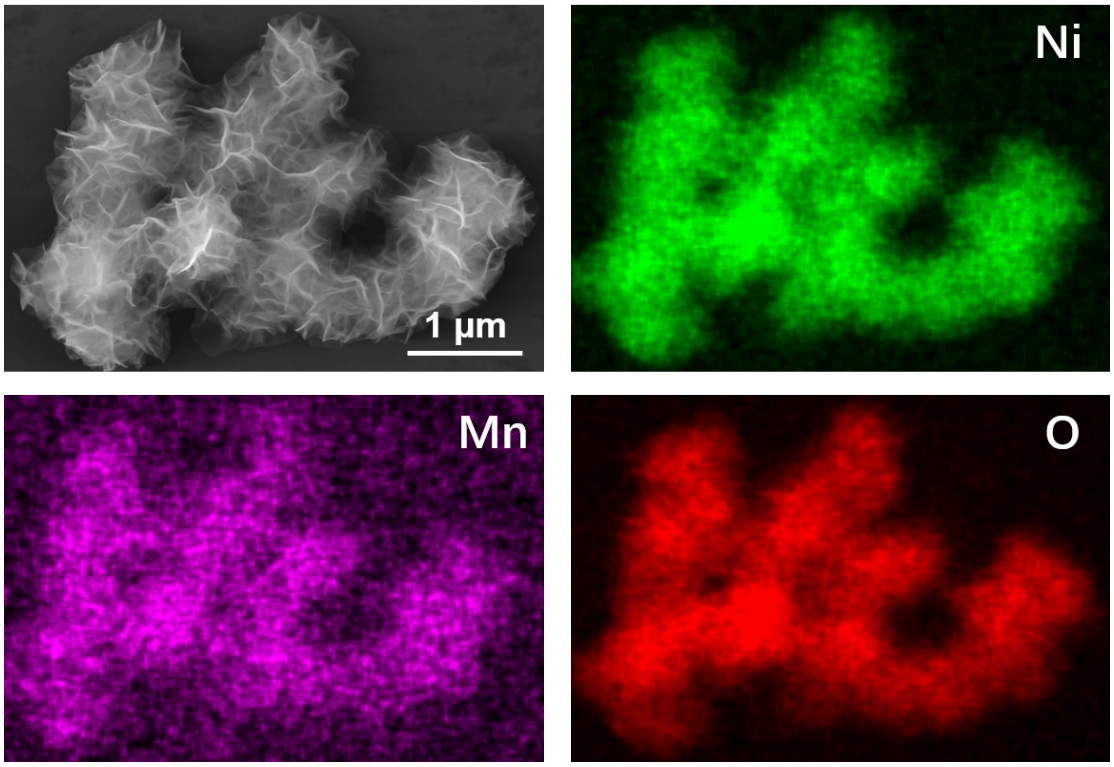

Figure S1. EDS mappings of NiMn-LDH

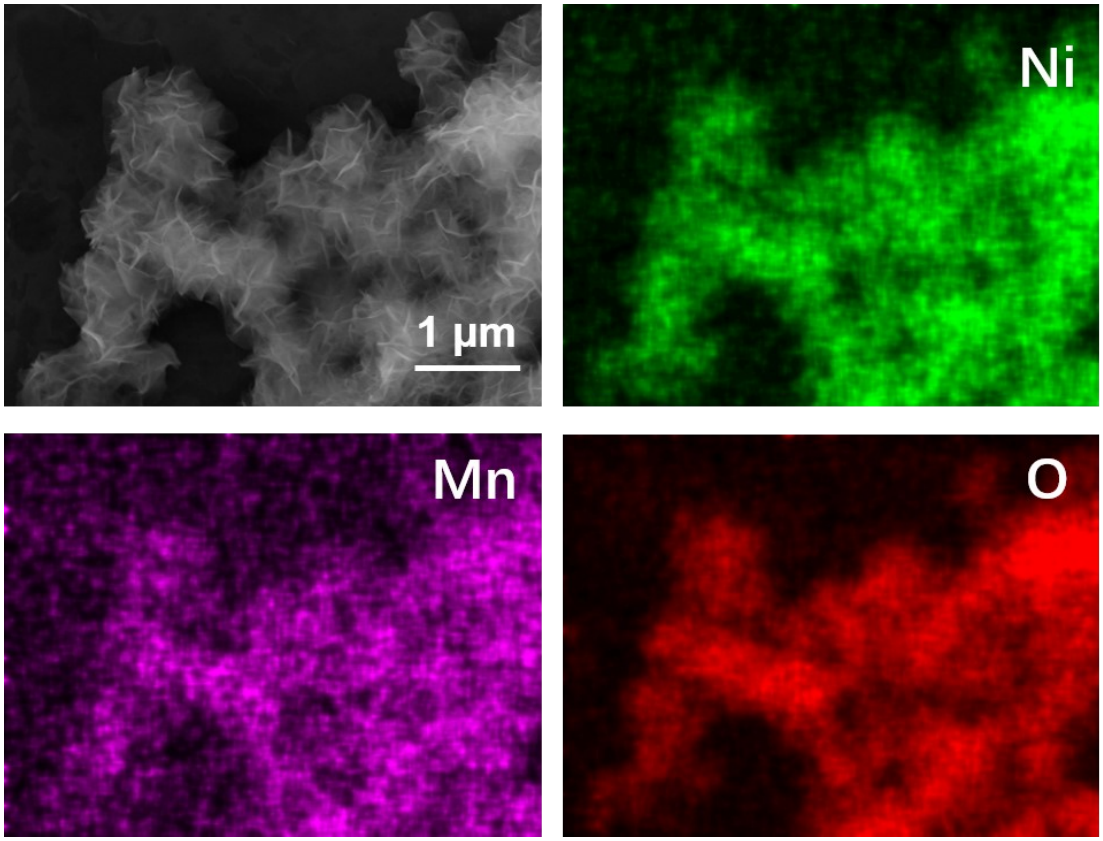

Figure S2. EDS mappings of LDH-O

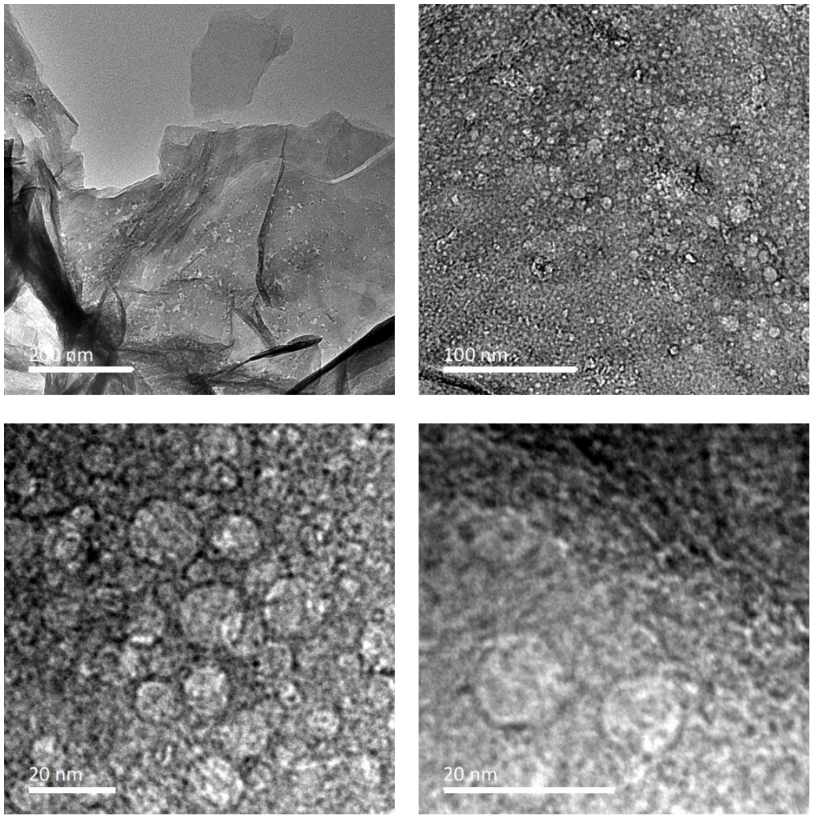

Figure S3. a,b) TEM image of LDH-O; c,d) HRTEM image of LDH-O.

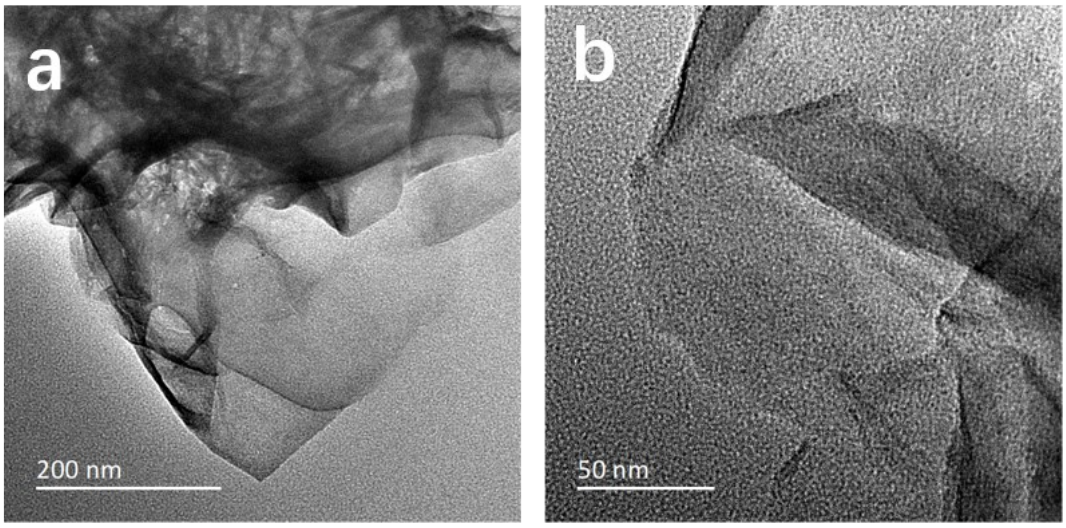

Figure S4. a) TEM image of NiMn-LDH; b) HRTEM image of NiMn-LDH.

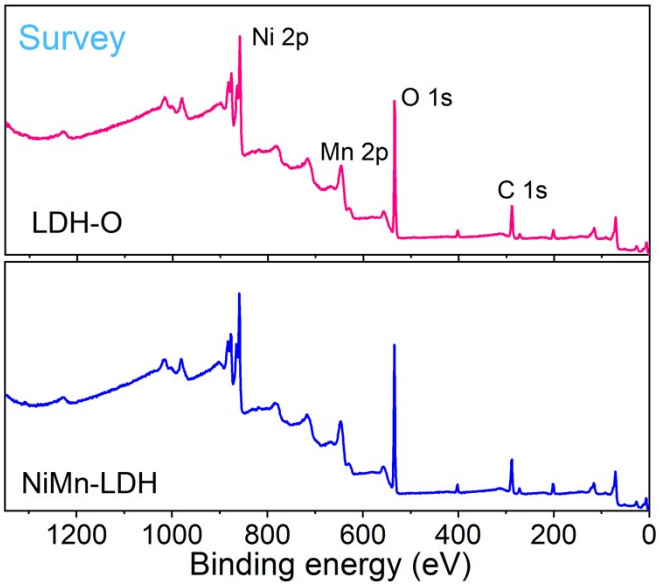

Figure S5. XPS survey spectra of NiMn-LDH and LDH-O

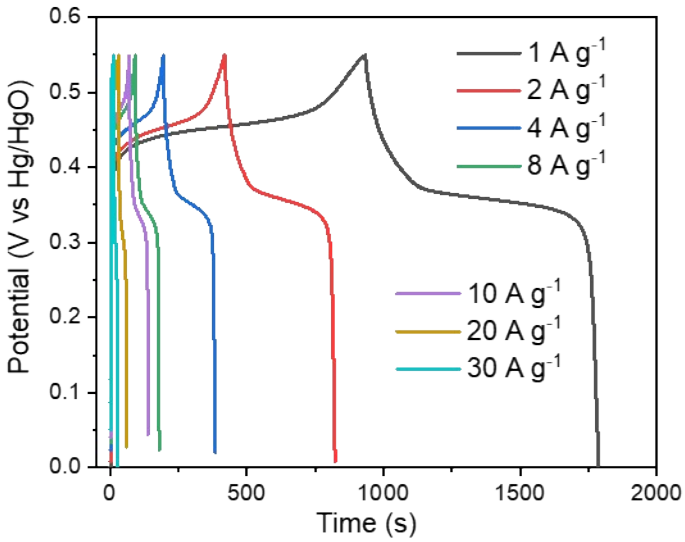

Figure S6. GCD curves of NiO_xH_y at different constant current densities.

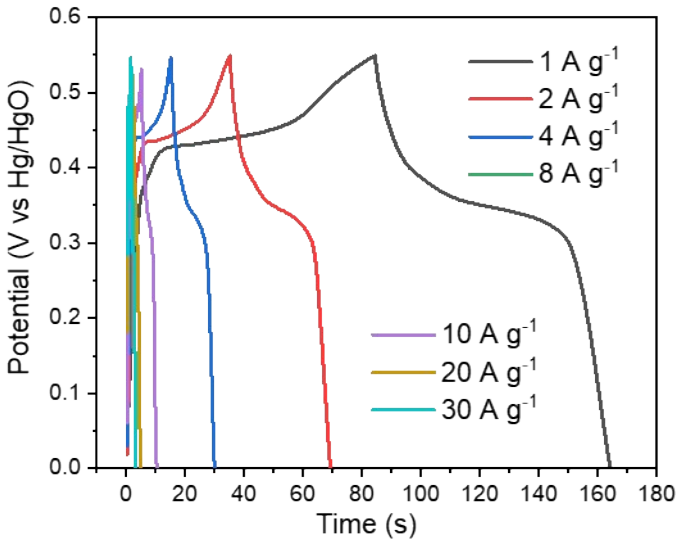

Figure S7. GCD curves of MnO_xH_y at different constant current densities.

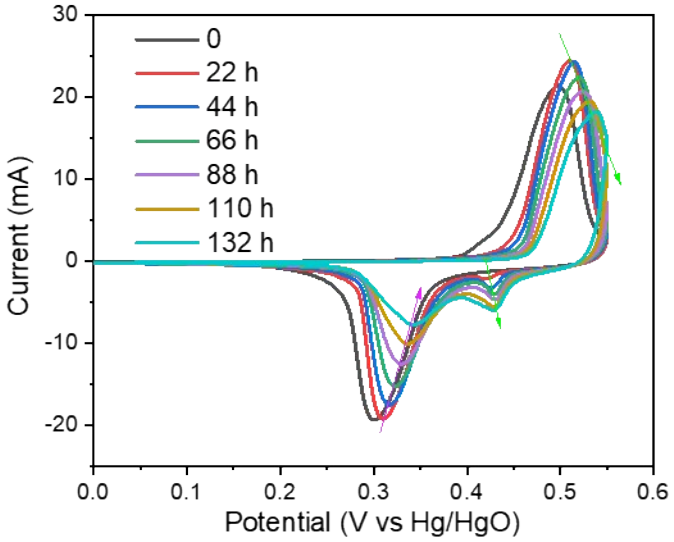

Figure S8. CV curves of the NiO_xH_y electrode at a scan rate of 1 mV s^{-1} in 2 M KOH.

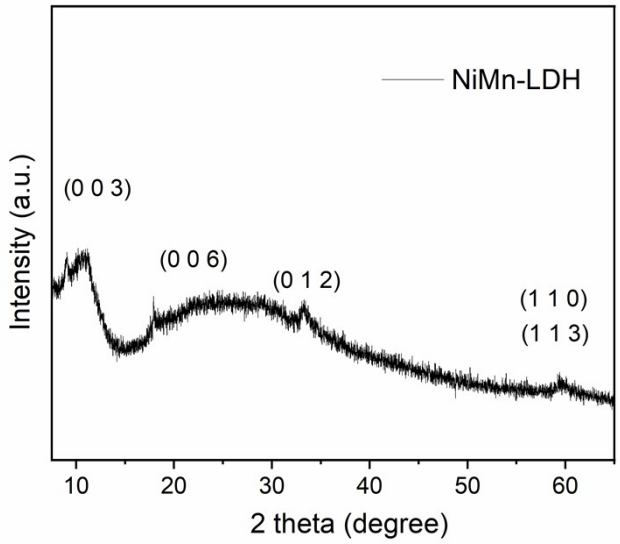

Figure S9. XRD patterns of NiMn-LDH after the phase change.

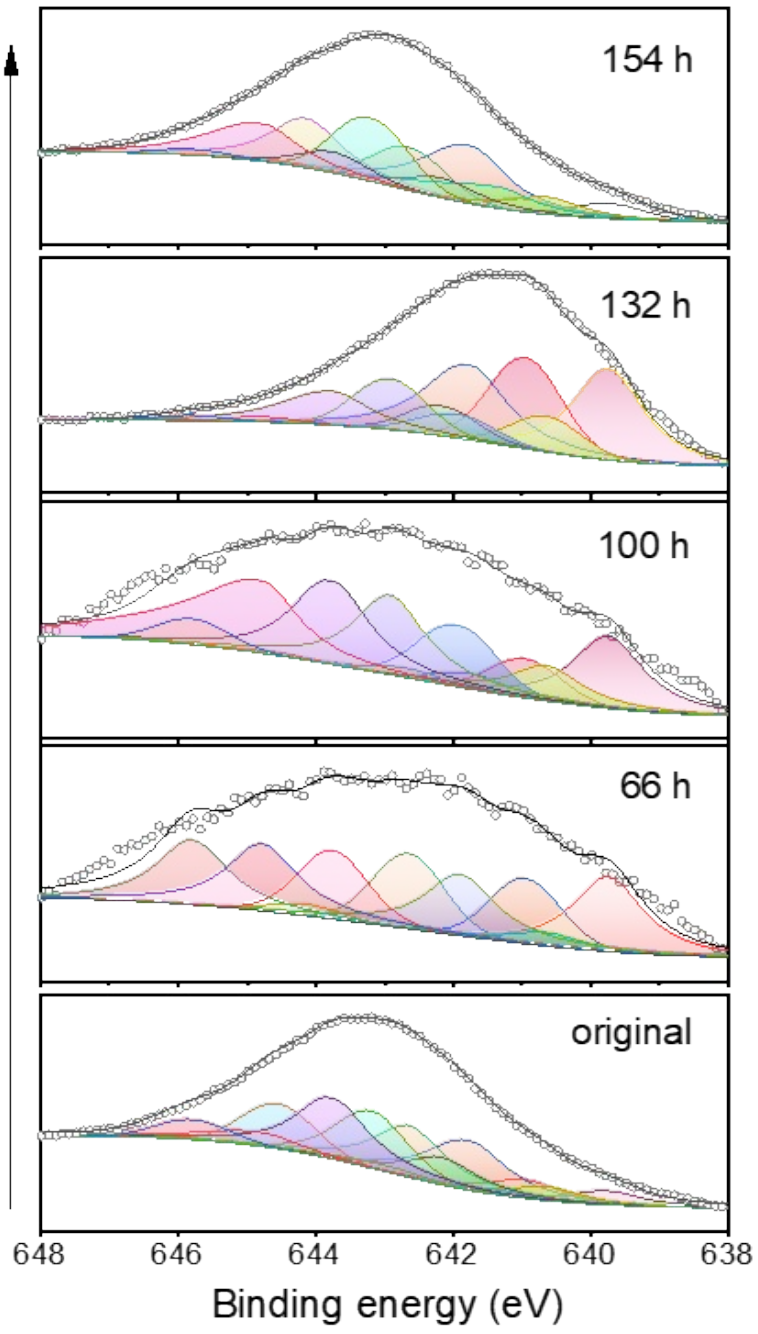

Figure S10. XPS Mn 2p3/2 spectra of NiMn-LDH during the cycling.

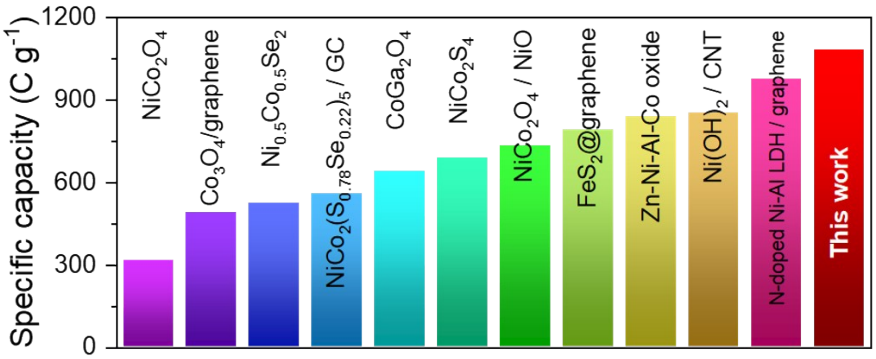

Figure S11. Comparison of specific capacity of various transition metal based materials.

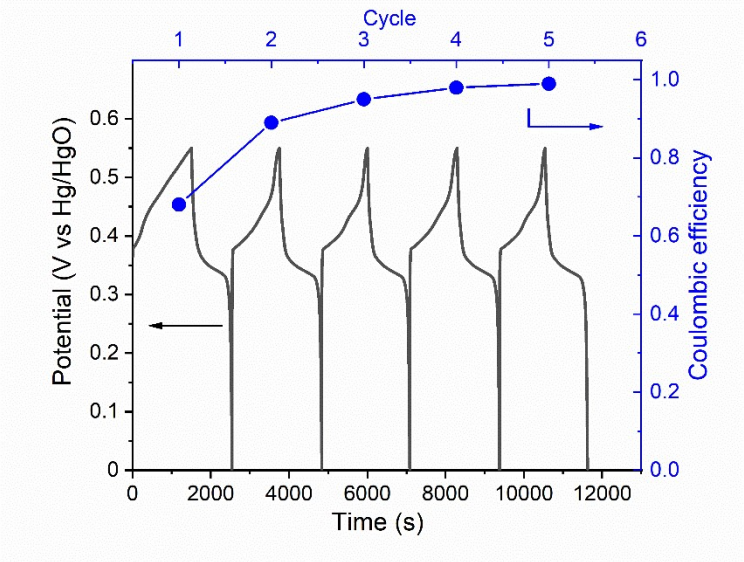

Figure S12. GCD curves and corresponding Coulombic efficiency of LDH-O for the first 5 cycles

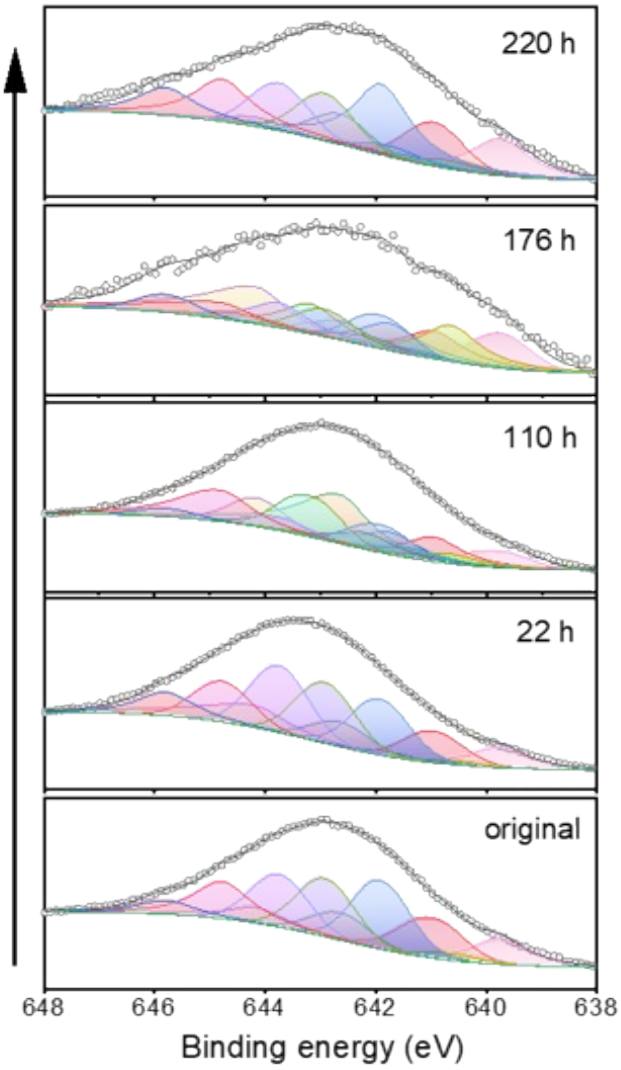

Figure S13. XPS Mn 2p3/2 spectra of NiMn-LDH during the cycling.

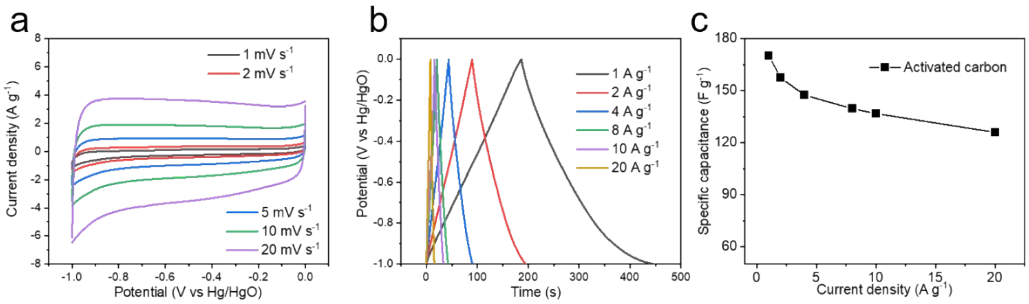

Figure S14. (a) CV curves of AC at scan rates 1, 2, 5, 10, and 20 mV s^{-1}. (b) Galvanostatic charge/discharge curves of AC at different constant current densities. (c) Specific capacity of AC as a function of the current densities calculated from the corresponding discharge curve for each current density.

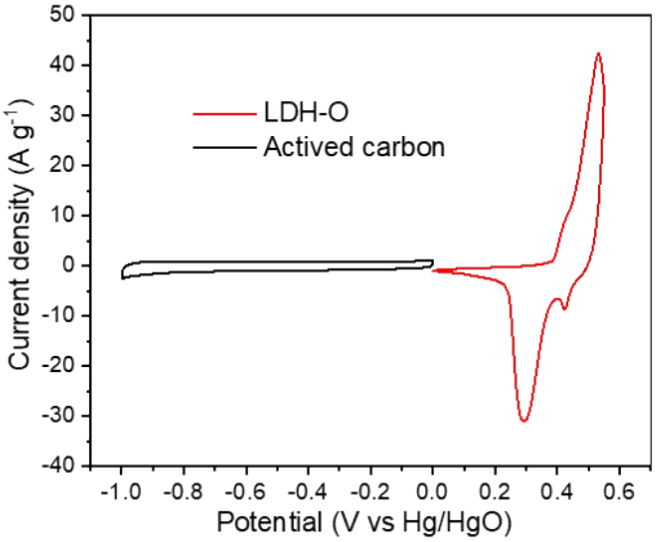

Figure S15. CV curves comparison between LDH-O positive electrode active material and activated carbon negative electrode material at 5 mV s^{-1}.

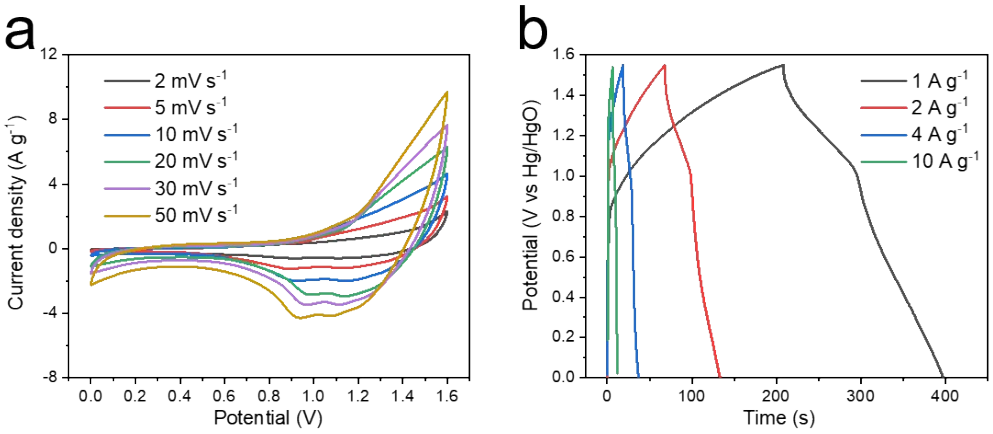

Figure S16. (a) CV curves of NiMn-LDH//AC at scan rates 2, 5, 10, 20, 30, and 50 mV s^{-1}. (b) Galvanostatic charge/discharge curves of NiMn-LDH//AC at different constant current densities.

Table S1. O1s peak parameters for NiMn-LDH and LDH-O.

	O 1s			OH^- ratio	OH^-/O^{2-}
Binding energy (eV)	530.8 O^{2-}	531.6 OH^-	532.9 H_2O		
NiMn-LDH	102386.59	266569.16	18449.5	68.8 %	2.6
LDH-O	44575.92	98461.52	8652.62	64.9 %	2.2

Table S2. Mn $2p_{3/2}$ peak parameters for NiMn-LDH and Ov-LDH.

			$Mn^{2+}(2p_{3/2})$			Sum
Binding energy (eV)	639.75	640.95	641.75	642.65	644.15	
NiMn-LDH	10379.69	14824.73	34705.29	33834.56	0	37.08 %
LDH-O	17455.41	26546.7	0	16512.44	12533.28	33.19 %
			Mn^{3+}(2p3/2)			Sum
Binding energy (eV)	640.65	641.35	642.16	643.18	644.55	
NiMn-LDH	9082.68	3617.02	18056.43	36349.84	23071.27	35.67 %
LDH-O	4312.75	585.18	0	303.25	0	2.36 %
			Mn^{4+}(2p3/2)			Sum
Binding energy (eV)	641.9	642.92	643.75	644.78	645.8	
NiMn-LDH	556.89	5928.46	40448.86	11635.51	10333.00	27.25 %
LDH-O	40574.27	34441.35	31013.64	26492.27	9289.25	64.44 %

Table S3. Mn $2p_{3/2}$ peak parameters for NiMn-LDH (66 h) and Ov-LDH (22 h) at the end of Stage I.

			$Mn^{2+}(2p_{3/2})$			Sum
Binding energy (eV)	639.75	640.95	641.75	642.65	644.15	
NiMn-LDH	10616.1	7612.95	14944.73	4810.29	1380.48	49.96 %
LDH-O	15119.14	20095.82	4082.86	15741.9	25601.27	33.38 %
			Mn^{3+}(2p3/2)			Sum
Binding energy (eV)	640.65	641.35	642.16	643.18	644.55	
NiMn-LDH	2232.82	0	338.1	0	0	3.07 %
LDH-O	2501.72	26.00	0	51.52	148.48	1.13 %
			Mn^{4+}(2p3/2)			Sum
Binding energy (eV)	641.9	642.92	643.75	644.78	645.8	
NiMn-LDH	9925.33	3677.07	8036.24	10693.02	9565.15	49.98 %
LDH-O	35534.42	38429.54	42036.36	25370.99	16839.85	65.49 %

Table S4. Mn $2p_{3/2}$ peak parameters for NiMn-LDH (100 h) and Ov-LDH (110 h) at the middle of Stage II.

			$Mn^{2+}(2p_{3/2})$			Sum
Binding energy (eV)	639.75	640.95	641.75	642.65	644.15	
NiMn-LDH	11129.17	4836.15	1978.99	1667.74	0	23.25 %
LDH-O	12861.72	13167.49	3297.44	9018.8	2710.3	31.41 %
			Mn^{3+}(2p3/2)			Sum
Binding energy (eV)	640.65	641.35	642.16	643.18	644.55	
NiMn-LDH	5906.4	759.14	601.6	0	561.25	9.28 %
LDH-O	2514.64	2342.25	942.77	0	0	4.44 %
			Mn^{4+}(2p3/2)			Sum
Binding energy (eV)	641.9	642.92	643.75	644.78	645.8	
NiMn-LDH	8367.22	13185.61	14212.12	17906.71	3245.39	67.47 %
LDH-O	28384.14	13933.24	14074.55	17062.14	10402.51	64.15 %

Table S5. Mn $2p_{3/2}$ peak parameters for NiMn-LDH (132 h) and Ov-LDH (176 h) at the middle of Stage III.

			$Mn^{2+}(2p_{3/2})$			Sum
Binding energy (eV)	639.75	640.95	641.75	642.65	644.15	
NiMn-LDH	43537.75	38628.01	44805.09	0	1248.71	59.07 %
LDH-O	3943.03	4185.5	4106.99	2896.79	7771.93	43.86 %
			Mn^{3+}(2p3/2)			Sum
Binding energy (eV)	640.65	641.35	642.16	643.18	644.55	
NiMn-LDH	15074.7	0	12671.31	573.76	1084.03	13.55 %
LDH-O	5427.38	822.64	1117.99	4500.56	1172.29	24.97 %
			Mn^{4+}(2p3/2)			Sum
Binding energy (eV)	641.9	642.92	643.75	644.78	645.8	
NiMn-LDH	10866.01	21705.99	21777.7	2472.45	2631.85	27.39 %
LDH-O	3933.19	3102.11	3728.2	3479.29	2033.81	31.17 %

Table S6. Mn $2p_{3/2}$ peak parameters for NiMn-LDH (154 h) and Ov-LDH (220 h) at the end of Stage III.

			$Mn^{2+}(2p_{3/2})$			Sum
Binding energy (eV)	639.75	640.95	641.75	642.65	644.15	
NiMn-LDH	7913.05	8403.65	42252.15	22126.33	31160.46	47.33 %
LDH-O	11842.61	18340.15	17064.56	45911.51	17519.39	48.78 %
			Mn^{3+}(2p3/2)			Sum
Binding energy (eV)	640.65	641.35	642.16	643.18	644.55	
NiMn-LDH	11348.73	21313.35	13063.16	33340.85	2773.26	34.63 %
LDH-O	7394.05	7625.93	12779.08	26780.24	0	24.06 %
			Mn^{4+}(2p3/2)			Sum
Binding energy (eV)	641.9	642.92	643.75	644.78	645.8	
NiMn-LDH	0	0	10955.39	28474.45	3214.79	18.04 %
LDH-O	17541.82	2345.29	8750.93	27937.61	5058.6	27.16 %

Table S7. Comparison of electrochemistry performance of various transition metal based materials.

Materials	Current density	Specific capacity	Cycles	CR	Electrolyte
$NiCo_2O_4$	1 A g^{-1}	315	50000	91.6 %	2 M KOH
$Ni_{0.5}Co_{0.5}Se_2$	1 A g^{-1}	524	3500	91 %	6 M KOH
$NiCo_2(S_{0.78}Se_{0.22})_5$/GC	1 A g^{-1}	561	2000	93.7 %	3 M KOH
$CoGa_2O_4$	1 A g^{-1}	642	20000	123 %	3 M KOH
$NiCo_2S_4$	1 A g^{-1}	689	10000	98.8 %	6 M KOH
$NiCo_2O_4$/NiO	1 A g^{-1}	732	3000	92.5 %	6 M KOH
FeS_2@graphene	3 A g^{-1}	793	5000	88 %	2 M KOH
Zn-Ni-Al-Co oxide	1 A g^{-1}	839	10000	90%	2 M KOH
$Ni(OH)_2$/CNT	2 A g^{-1}	854	5000	84 %	PVA-KOH
N-doped Ni-Al LDH / graphene	1 A g^{-1}	975	2000	80 %	6 M KOH
This work	1 A g^{-1}	1082	3000	85 %	2 M KOH